

The Inclusive Jet Cross Section in $\bar{p}p$ Collisions at $\sqrt{s} = 1.8$ TeV

B. Abbott,⁴⁰ M. Abolins,³⁷ V. Abramov,¹⁵ B.S. Acharya,⁸ I. Adam,³⁹ D.L. Adams,⁴⁸
M. Adams,²⁴ S. Ahn,²³ H. Aihara,¹⁷ G.A. Alves,² N. Amos,³⁶ E.W. Anderson,³⁰ R. Astur,⁴²
M.M. Baarmand,⁴² V.V. Babintsev,¹⁵ L. Babukhadia,¹⁶ A. Baden,³³ V. Balamurali,²⁸
B. Baldin,²³ S. Banerjee,⁸ J. Bantly,⁴⁵ E. Barberis,¹⁷ P. Baringer,³¹ J.F. Bartlett,²³
A. Belyaev,¹⁴ S.B. Beri,⁶ I. Bertram,²⁶ V.A. Bezzubov,¹⁵ P.C. Bhat,²³ V. Bhatnagar,⁶
M. Bhattacharjee,⁴² N. Biswas,²⁸ G. Blazey,²⁵ S. Blessing,²¹ P. Bloom,¹⁸ A. Boehnlein,²³
N.I. Bojko,¹⁵ F. Borchering,²³ C. Boswell,²⁰ A. Brandt,²³ R. Breedon,¹⁸ R. Brock,³⁷
A. Bross,²³ D. Buchholz,²⁶ V.S. Burtovoi,¹⁵ J.M. Butler,³⁴ W. Carvalho,² D. Casey,³⁷
Z. Casilum,⁴² H. Castilla-Valdez,¹¹ D. Chakraborty,⁴² S.-M. Chang,³⁵ S.V. Chekulaev,¹⁵
L.-P. Chen,¹⁷ W. Chen,⁴² S. Choi,¹⁰ S. Chopra,³⁶ B.C. Choudhary,²⁰ J.H. Christenson,²³
M. Chung,²⁴ D. Claes,³⁸ A.R. Clark,¹⁷ W.G. Cobau,³³ J. Cochran,²⁰ L. Coney,²⁸
W.E. Cooper,²³ C. Cretsinger,⁴¹ D. Cullen-Vidal,⁴⁵ M.A.C. Cummings,²⁵ D. Cutts,⁴⁵
O.I. Dahl,¹⁷ K. Davis,¹⁶ K. De,⁴⁶ K. Del Signore,³⁶ M. Demarteau,²³ D. Denisov,²³
S.P. Denisov,¹⁵ H.T. Diehl,²³ M. Diesburg,²³ G. Di Loreto,³⁷ P. Draper,⁴⁶ Y. Ducros,⁵
L.V. Dudko,¹⁴ S.R. Dugad,⁸ A. Dyshkant,¹⁵ D. Edmunds,³⁷ J. Ellison,²⁰ V.D. Elvira,⁴²
R. Engelmann,⁴² S. Eno,³³ G. Eppley,⁴⁸ P. Ermolov,¹⁴ O.V. Eroshin,¹⁵ V.N. Evdokimov,¹⁵
T. Fahland,¹⁹ M.K. Fatyga,⁴¹ S. Feher,²³ D. Fein,¹⁶ T. Ferbel,⁴¹ G. Finocchiaro,⁴²
H.E. Fisk,²³ Y. Fisyak,⁴³ E. Flattum,²³ G.E. Forden,¹⁶ M. Fortner,²⁵ K.C. Frame,³⁷
S. Fuess,²³ E. Gallas,⁴⁶ A.N. Galyaev,¹⁵ P. Garton,²⁰ V. Gavrilov,¹³ T.L. Geld,³⁷
R.J. Genik II,³⁷ K. Genser,²³ C.E. Gerber,²³ Y. Gershtein,¹³ B. Gibbard,⁴³ B. Gobbi,²⁶
B. Gómez,⁴ G. Gómez,³³ P.I. Goncharov,¹⁵ J.L. González Solís,¹¹ H. Gordon,⁴³ L.T. Goss,⁴⁷
K. Gounder,²⁰ A. Goussiou,⁴² N. Graf,⁴³ P.D. Grannis,⁴² D.R. Green,²³ H. Greenlee,²³
S. Grinstein,¹ P. Grudberg,¹⁷ S. Grünendahl,²³ G. Guglielmo,⁴⁴ J.A. Guida,¹⁶ J.M. Guida,⁴⁵
A. Gupta,⁸ S.N. Gurzhiev,¹⁵ G. Gutierrez,²³ P. Gutierrez,⁴⁴ N.J. Hadley,³³ H. Haggerty,²³
S. Hagopian,²¹ V. Hagopian,²¹ K.S. Hahn,⁴¹ R.E. Hall,¹⁹ P. Hanlet,³⁵ S. Hansen,²³
J.M. Hauptman,³⁰ D. Hedin,²⁵ A.P. Heinson,²⁰ U. Heintz,²³ R. Hernández-Montoya,¹¹
T. Heuring,²¹ R. Hirosky,²⁴ J.D. Hobbs,⁴² B. Hoeneisen,^{4,*} J.S. Hoftun,⁴⁵ F. Hsieh,³⁶
Ting Hu,⁴² Tong Hu,²⁷ T. Huehn,²⁰ A.S. Ito,²³ E. James,¹⁶ J. Jaques,²⁸ S.A. Jerger,³⁷
R. Jesik,²⁷ T. Joffe-Minor,²⁶ K. Johns,¹⁶ M. Johnson,²³ A. Jonckheere,²³ M. Jones,²²
H. Jöstlein,²³ S.Y. Jun,²⁶ C.K. Jung,⁴² S. Kahn,⁴³ G. Kalbfleisch,⁴⁴ D. Karmanov,¹⁴
D. Karmgard,²¹ R. Kehoe,²⁸ M.L. Kelly,²⁸ S.K. Kim,¹⁰ B. Klima,²³ C. Klopfenstein,¹⁸
W. Ko,¹⁸ J.M. Kohli,⁶ D. Koltick,²⁹ A.V. Kostitskiy,¹⁵ J. Kotcher,⁴³ A.V. Kotwal,³⁹
A.V. Kozelov,¹⁵ E.A. Kozlovsky,¹⁵ J. Krane,³⁸ M.R. Krishnaswamy,⁸ S. Krzywdzinski,²³
S. Kuleshov,¹³ S. Kunori,³³ F. Landry,³⁷ G. Landsberg,⁴⁵ B. Lauer,³⁰ A. Leflat,¹⁴ J. Li,⁴⁶
Q.Z. Li-Demarteau,²³ J.G.R. Lima,³ D. Lincoln,²³ S.L. Linn,²¹ J. Linnemann,³⁷
R. Lipton,²³ F. Lobkowicz,⁴¹ S.C. Loken,¹⁷ A. Lucotte,⁴² L. Lueking,²³ A.L. Lyon,³³
A.K.A. Maciel,² R.J. Madaras,¹⁷ R. Madden,²¹ L. Magaña-Mendoza,¹¹ V. Manankov,¹⁴
S. Mani,¹⁸ H.S. Mao,^{23,†} R. Markeloff,²⁵ T. Marshall,²⁷ M.I. Martin,²³ K.M. Mauritz,³⁰
B. May,²⁶ A.A. Mayorov,¹⁵ R. McCarthy,⁴² J. McDonald,²¹ T. McKibben,²⁴ J. McKinley,³⁷
T. McMahan,⁴⁴ H.L. Melanson,²³ M. Merkin,¹⁴ K.W. Merritt,²³ C. Miao,⁴⁵ H. Miettinen,⁴⁸
A. Mincer,⁴⁰ C.S. Mishra,²³ N. Mokhov,²³ N.K. Mondal,⁸ H.E. Montgomery,²³ P. Mooney,⁴
M. Mostafa,¹ H. da Motta,² C. Murphy,²⁴ F. Nang,¹⁶ M. Narain,²³ V.S. Narasimham,⁸

A. Narayanan,¹⁶ H.A. Neal,³⁶ J.P. Negret,⁴ P. Nemethy,⁴⁰ D. Norman,⁴⁷ L. Oesch,³⁶
V. Oguri,³ E. Oliveira,² E. Oltman,¹⁷ N. Oshima,²³ D. Owen,³⁷ P. Padley,⁴⁸ A. Para,²³
Y.M. Park,⁹ R. Partridge,⁴⁵ N. Parua,⁸ M. Paterno,⁴¹ B. Pawlik,¹² J. Perkins,⁴⁶
M. Peters,²² R. Piegaiia,¹ H. Piekarz,²¹ Y. Pischalnikov,²⁹ B.G. Pope,³⁷ H.B. Prosper,²¹
S. Protopopescu,⁴³ J. Qian,³⁶ P.Z. Quintas,²³ R. Raja,²³ S. Rajagopalan,⁴³ O. Ramirez,²⁴
S. Reucroft,³⁵ M. Rijssenbeek,⁴² T. Rockwell,³⁷ M. Roco,²³ P. Rubinov,²⁶ R. Ruchti,²⁸
J. Rutherford,¹⁶ A. Sánchez-Hernández,¹¹ A. Santoro,² L. Sawyer,³² R.D. Schamberger,⁴²
H. Schellman,²⁶ J. Sculli,⁴⁰ E. Shabalina,¹⁴ C. Shaffer,²¹ H.C. Shankar,⁸ R.K. Shivpuri,⁷
M. Shupe,¹⁶ H. Singh,²⁰ J.B. Singh,⁶ V. Sirotenko,²⁵ E. Smith,⁴⁴ R.P. Smith,²³ R. Snihur,²⁶
G.R. Snow,³⁸ J. Snow,⁴⁴ S. Snyder,⁴³ J. Solomon,²⁴ M. Sosebee,⁴⁶ N. Sotnikova,¹⁴
M. Souza,² A.L. Spadafora,¹⁷ G. Steinbrück,⁴⁴ R.W. Stephens,⁴⁶ M.L. Stevenson,¹⁷
D. Stewart,³⁶ F. Stichelbaut,⁴² D. Stoker,¹⁹ V. Stolin,¹³ D.A. Stoyanova,¹⁵ M. Strauss,⁴⁴
K. Streets,⁴⁰ M. Strovink,¹⁷ A. Sznajder,² P. Tamburello,³³ J. Tarazi,¹⁹ M. Tartaglia,²³
T.L.T. Thomas,²⁶ J. Thompson,³³ T.G. Trippe,¹⁷ P.M. Tuts,³⁹ V. Vaniev,¹⁵ N. Varelas,²⁴
E.W. Varnes,¹⁷ D. Vititoe,¹⁶ A.A. Volkov,¹⁵ A.P. Vorobiev,¹⁵ H.D. Wahl,²¹ G. Wang,²¹
J. Warchol,²⁸ G. Watts,⁴⁵ M. Wayne,²⁸ H. Weerts,³⁷ A. White,⁴⁶ J.T. White,⁴⁷
J.A. Wightman,³⁰ S. Willis,²⁵ S.J. Wimpenny,²⁰ J.V.D. Wirjawan,⁴⁷ J. Womersley,²³
E. Won,⁴¹ D.R. Wood,³⁵ Z. Wu,^{23,†} H. Xu,⁴⁵ R. Yamada,²³ P. Yamin,⁴³ T. Yasuda,³⁵
P. Yepes,⁴⁸ K. Yip,²³ C. Yoshikawa,²² S. Youssef,²¹ J. Yu,²³ Y. Yu,¹⁰ B. Zhang,^{23,†}
Y. Zhou,^{23,†} Z. Zhou,³⁰ Z.H. Zhu,⁴¹ M. Zielinski,⁴¹ D. Zieminska,²⁷ A. Zieminski,²⁷
E.G. Zverev,¹⁴ and A. Zylberstejn⁵

(DØ Collaboration)

¹ *Universidad de Buenos Aires, Buenos Aires, Argentina*

² *LAFEX, Centro Brasileiro de Pesquisas Físicas, Rio de Janeiro, Brazil*

³ *Universidade do Estado do Rio de Janeiro, Rio de Janeiro, Brazil*

⁴ *Universidad de los Andes, Bogotá, Colombia*

⁵ *DAPNIA/Service de Physique des Particules, CEA, Saclay, France*

⁶ *Panjab University, Chandigarh, India*

⁷ *Delhi University, Delhi, India*

⁸ *Tata Institute of Fundamental Research, Mumbai, India*

⁹ *Kyungshung University, Pusan, Korea*

¹⁰ *Seoul National University, Seoul, Korea*

¹¹ *CINVESTAV, Mexico City, Mexico*

¹² *Institute of Nuclear Physics, Kraków, Poland*

¹³ *Institute for Theoretical and Experimental Physics, Moscow, Russia*

¹⁴ *Moscow State University, Moscow, Russia*

¹⁵ *Institute for High Energy Physics, Protvino, Russia*

¹⁶ *University of Arizona, Tucson, Arizona 85721*

¹⁷ *Lawrence Berkeley National Laboratory and University of California, Berkeley, California 94720*

¹⁸ *University of California, Davis, California 95616*

¹⁹ *University of California, Irvine, California 92697*

²⁰ *University of California, Riverside, California 92521*

- ²¹ *Florida State University, Tallahassee, Florida 32306*
²² *University of Hawaii, Honolulu, Hawaii 96822*
²³ *Fermi National Accelerator Laboratory, Batavia, Illinois 60510*
²⁴ *University of Illinois at Chicago, Chicago, Illinois 60607*
²⁵ *Northern Illinois University, DeKalb, Illinois 60115*
²⁶ *Northwestern University, Evanston, Illinois 60208*
²⁷ *Indiana University, Bloomington, Indiana 47405*
²⁸ *University of Notre Dame, Notre Dame, Indiana 46556*
²⁹ *Purdue University, West Lafayette, Indiana 47907*
³⁰ *Iowa State University, Ames, Iowa 50011*
³¹ *University of Kansas, Lawrence, Kansas 66045*
³² *Louisiana Tech University, Ruston, Louisiana 71272*
³³ *University of Maryland, College Park, Maryland 20742*
³⁴ *Boston University, Boston, Massachusetts 02215*
³⁵ *Northeastern University, Boston, Massachusetts 02115*
³⁶ *University of Michigan, Ann Arbor, Michigan 48109*
³⁷ *Michigan State University, East Lansing, Michigan 48824*
³⁸ *University of Nebraska, Lincoln, Nebraska 68588*
³⁹ *Columbia University, New York, New York 10027*
⁴⁰ *New York University, New York, New York 10003*
⁴¹ *University of Rochester, Rochester, New York 14627*
⁴² *State University of New York, Stony Brook, New York 11794*
⁴³ *Brookhaven National Laboratory, Upton, New York 11973*
⁴⁴ *University of Oklahoma, Norman, Oklahoma 73019*
⁴⁵ *Brown University, Providence, Rhode Island 02912*
⁴⁶ *University of Texas, Arlington, Texas 76019*
⁴⁷ *Texas A&M University, College Station, Texas 77843*
⁴⁸ *Rice University, Houston, Texas 77005*

Abstract

We have made a precise measurement of the central inclusive jet cross section at $\sqrt{s} = 1.8$ TeV. The measurement is based on an integrated luminosity of 92 pb^{-1} collected at the Fermilab Tevatron $p\bar{p}$ Collider with the DØ detector. The cross section, reported as a function of jet transverse energy ($E_T \geq 60$ GeV) in the pseudorapidity interval $|\eta| \leq 0.5$, is in good agreement with predictions from next-to-leading order quantum chromodynamics.

Within the framework of quantum chromodynamics (QCD), inelastic scattering between a proton and an antiproton can be described as an elastic collision between a single proton constituent and a single antiproton constituent. These constituents are often referred to as partons. After the collision, the outgoing partons manifest themselves as localized streams of particles or “jets”. Predictions for the inclusive jet cross section are given by the folding of parton scattering cross sections with experimentally determined parton distribution functions (pdf’s). These predictions have recently improved with next-to-leading order (NLO) QCD scattering calculations [1-3] and new, accurately measured pdf’s [4,5]. We measure the cross section for the production of jets as a function of the jet energy in the plane transverse to the incident beams, E_T . The measurement is based on an integrated luminosity of 92 pb^{-1} of $p\bar{p}$ collisions collected with the DØ detector [6] at the Fermilab Tevatron Collider. Measurements of inclusive jet production with smaller integrated luminosity have been performed previously by the UA2 and CDF collaborations [7,8]. The cross section measurement presented here allows a stringent test of QCD, with a total uncertainty substantially reduced relative to previous results.

Jet detection in the DØ detector utilizes primarily the uranium-liquid argon calorimeters which have full coverage for pseudorapidity $|\eta| \leq 4.1$ ($\eta = -\ln(\tan(\theta/2))$, where θ is the polar angle relative to the proton beam). The calorimeter is segmented into towers of $\Delta\eta \times \Delta\phi = 0.1 \times 0.1$, where ϕ is the azimuthal angle.

Initial event selection occurred in two hardware trigger stages and a software stage. The first hardware trigger selected an inelastic $p\bar{p}$ collision – indicated by signals from the trigger hodoscopes located near the beams on either side of the interaction region. The next stage required transverse energy above a preset threshold in calorimeter trigger tiles of $\Delta\eta \times \Delta\phi = 0.8 \times 1.6$. Selected events were digitized and sent to an array of processors. Jet candidates were then reconstructed with a cone algorithm and the entire event recorded if any jet E_T exceeded a specified threshold. For software jet thresholds of 30, 50, 85, and 115 GeV, integrated luminosities of 0.34, 4.6, 55, and 92 pb^{-1} , respectively, were accumulated during a 1994–1995 data run. The two lowest E_T triggers required a single proton-antiproton interaction within the beam crossing as signaled by timing information in the trigger hodoscopes.

Jets were reconstructed offline using an iterative fixed-cone algorithm with a cone radius of $\mathcal{R}=0.7$ in η - ϕ space [9]. Background from isolated noisy calorimeter cells and accelerator beam losses which mimicked jets were eliminated with quality cuts [10]. Background events from cosmic ray bremsstrahlung or misvertexed events were eliminated by requiring the missing transverse energy in each event to be less than the larger of 30 GeV or $0.3E_T^{\text{max}}$, where E_T^{max} is the E_T of the leading jet. Residual jet contamination is less than 1% at all E_T , based on event simulations with superimposed calorimeter noise distributions and on visual scanning of jet candidates with E_T greater than 350 GeV. The jet selection efficiency for $|\eta| \leq 0.7$ has been measured as a function of jet E_T and found to be $(97 \pm 1)\%$ below 250 GeV and $(95 \pm 2)\%$ at 400 GeV.

At high instantaneous luminosity, more than one interaction in a single beam crossing is probable ($\sim 20\%$ for this data set). The event vertex was reconstructed using data from the central tracking system. For events with multiple vertices, the two vertices with the largest number of tracks were retained. Due to fluctuations of jet charged-particle multiplicity, an additional parameter was used to select the vertex. If an event had more than one vertex,

the quantity $S_T = |\Sigma \vec{E}_T^{\text{jet}}|$ was calculated for both vertices. The vertex with the smaller S_T was selected as the event vertex and used to calculate jet E_T and η . The selected vertex was required to be within 50 cm of the detector center. This last requirement retained $(90\pm 1)\%$ of the events, independent of jet E_T .

The transverse energy of each jet was corrected for the underlying event, additional interactions, noise from uranium decay, the fraction of particle energy showered outside of the reconstruction cone, detector uniformity, and detector hadronic response. A complete discussion of the jet energy scale calibration can be found in Ref. [11]. For $|\eta| \leq 0.5$, the mean total correction factor for jet energy is 1.154 ± 0.017 [1.118 ± 0.023] at 100 GeV [400 GeV].

The inclusive jet cross section was computed in contiguous ranges of E_T using data from the four trigger sets. The spectrum includes data from the 30 GeV trigger between 60–90 GeV, from the 50 GeV E_T trigger between 90–130 GeV, then from the 85 GeV trigger between 130–170 GeV, and above 170 GeV from the 115 GeV trigger. The single interaction requirement on the two lowest- E_T triggers introduced an inefficiency which was corrected by matching the 50 GeV trigger cross section to the 85 GeV trigger cross section above 130 GeV, where both triggers are fully efficient. This introduces an additional 1.1% luminosity uncertainty to the 50 GeV trigger set. A similar matching between the lowest- E_T trigger and the 50 GeV trigger introduces another 1.4% uncertainty for the lower set, which is added in quadrature to the 1.1% matching uncertainty.

The steep E_T spectrum is distorted by jet energy resolution. At all E_T , the resolution (measured by balancing E_T in jet events) is well described by a gaussian distribution; at 100 GeV the standard deviation is 7 GeV. The distortion was corrected by assuming an ansatz function $(AE_T^{-B}) \cdot (1 - 2E_T/\sqrt{s})^C$, smearing it with the measured resolution, and comparing the smeared result with the measured cross section. The procedure was repeated by varying parameters A , B , and C until the best fit was found between the observed cross section and the smeared trial spectrum. The ratio of the initial ansatz to the smeared ansatz was used to correct the cross section on a bin-by-bin basis [12]. The resolution correction reduces the observed cross section by $(13\pm 3)\%$ [$(8\pm 2)\%$] at 60 GeV [400 GeV].

The resulting inclusive jet cross section for $|\eta| \leq 0.5$, shown in Fig. 1, has been averaged over each E_T bin (ΔE_T) and over the central unit of rapidity ($\Delta\eta=1$). This bin-averaged double differential cross section, $\langle d^2\sigma/(dE_T d\eta) \rangle$, was calculated as $N/(\Delta E_T \Delta\eta \epsilon \mathcal{L})$ where N is the total number of jets observed in the bin, ϵ is the selection efficiency as a function of E_T , and \mathcal{L} the integrated luminosity associated with the trigger set. The cross section is consistent with a preliminary measurement from a smaller 1992–1993 data set [10].

Figure 1 also shows a theoretical prediction for the cross section from the NLO event generator JETRAD [3]. There is good agreement over seven orders of magnitude. Inputs to the NLO calculation are the renormalization scale μ (always chosen to equal the factorization scale), the parton distribution function (pdf), and the parton clustering algorithm. For the calculation shown here, $\mu = 0.5E_T^{\text{max}}$ and the pdf is CTEQ3M [4]. Partons separated by less than $\mathcal{R}_{\text{sep}}=1.3\mathcal{R}$ were clustered if they were also within $\mathcal{R}=0.7$ of their E_T -weighted η - ϕ centroid. This choice of \mathcal{R}_{sep} is discussed in Ref. [9]. Variations in the predicted cross section due to the input choices are approximately 30% [13].

The data in Fig. 1 have an overall luminosity uncertainty of 6.1%. The data are plotted at the E_T value for which a smooth function describing the cross section is equal to the average cross section in the bin. The band shows the total systematic uncertainty as a function of

TABLE I. The $|\eta| < 0.5$ cross section.

Plotted E_T (GeV)	Bin Range (GeV)	Cross Sec. \pm Stat. (fb/GeV)	Sys. Uncer.(%)
64.6	60 – 70	$(6.59 \pm 0.04) \times 10^6$	± 8
74.6	70 – 80	$(2.89 \pm 0.03) \times 10^6$	± 8
84.7	80 – 90	$(1.41 \pm 0.02) \times 10^6$	± 8
94.7	90 – 100	$(7.07 \pm 0.04) \times 10^5$	± 8
104.7	100 – 110	$(3.88 \pm 0.03) \times 10^5$	± 8
114.8	110 – 120	$(2.21 \pm 0.02) \times 10^5$	± 8
124.8	120 – 130	$(1.27 \pm 0.02) \times 10^5$	± 8
134.8	130 – 140	$(7.70 \pm 0.04) \times 10^4$	± 8
144.8	140 – 150	$(4.86 \pm 0.03) \times 10^4$	± 8
154.8	150 – 160	$(3.07 \pm 0.02) \times 10^4$	+9, – 8
164.8	160 – 170	$(2.00 \pm 0.02) \times 10^4$	± 9
174.8	170 – 180	$(1.34 \pm 0.01) \times 10^4$	± 9
184.8	180 – 190	$(9.12 \pm 0.10) \times 10^3$	± 9
194.8	190 – 200	$(6.15 \pm 0.09) \times 10^3$	+10, – 9
204.8	200 – 210	$(4.29 \pm 0.07) \times 10^3$	± 10
214.8	210 – 220	$(2.93 \pm 0.06) \times 10^3$	+11, – 10
224.8	220 – 230	$(2.14 \pm 0.05) \times 10^3$	+11, – 10
239.4	230 – 250	$(1.30 \pm 0.03) \times 10^3$	± 11
259.4	250 – 270	$(6.54 \pm 0.20) \times 10^2$	+12, – 11
279.5	270 – 290	$(3.77 \pm 0.15) \times 10^2$	+13, – 12
303.9	290 – 320	$(1.79 \pm 0.08) \times 10^2$	+15, – 13
333.9	320 – 350	$(6.82 \pm 0.52) \times 10^1$	+17, – 15
375.7	350 – 410	$(1.89 \pm 0.19) \times 10^1$	+20, – 17
461.1	410 – 560	$(1.24 \pm 0.31) \times 10^0$	+30, – 26

E_T . Listed in Table I are the plotted values of E_T , the E_T ranges, the cross section, and the statistical and systematic uncertainty. The tabulated systematic uncertainties include jet and event selection, unsmearing, relative luminosity, and energy scale uncertainties added in quadrature. The 6.1% luminosity uncertainty is not included.

Figure 2 shows the various uncertainties for the $|\eta| \leq 0.5$ cross section. Each curve represents the average of the nearly symmetric upper and lower uncertainties. The uncertainty attributed to the energy scale varies from 8% at low E_T to 30% at 450 GeV. This contribution dominates all other sources of uncertainty, except at low E_T , where the 6.1% luminosity uncertainty is of comparable magnitude.

The $|\eta| \leq 0.5$ region provides our optimum test for departures of data from NLO QCD. In this region, the detector is uniformly thick (seven or more interaction lengths with no gaps) and both jet resolution and calibration are precise. Also, jet production from the scattering of possible constituents within quarks is largest for $\eta = 0$, relative to standard QCD predictions [14]. For comparison to Ref. [8], we have also carried out a similar analysis in the region $0.1 \leq |\eta| \leq 0.7$.

Figure 3 shows the ratios $(D - T)/T$ for the data (D) and JETRAD NLO theoretical (T)

TABLE II. Correlations of the total uncertainty in the cross section.

$E_T(\text{GeV})$	64.6	104.7	204.8	303.9	461.1
64.6	1.00	0.96	0.85	0.71	0.40
104.7	0.96	1.00	0.92	0.79	0.46
204.8	0.85	0.92	1.00	0.91	0.61
303.9	0.71	0.79	0.91	1.00	0.67
461.1	0.40	0.46	0.61	0.67	1.00

predictions based on the CTEQ3M, CTEQ4M and MRST pdf's [4,5] for $|\eta| \leq 0.5$. Given the experimental and theoretical uncertainties, the prediction is in good agreement with the data; in particular, the data above 350 GeV show no indication of an excess relative to QCD.

The data and theory can be compared quantitatively with a $\chi^2 = \sum_{i,j} (D_i - T_i)(C^{-1})_{ij}(D_j - T_j)$ test incorporating the uncertainty covariance matrix C . Here D_i and T_i represent the i -th data and theory points, respectively. The elements C_{ij} are constructed by analyzing the mutual correlation of the uncertainties in Fig. 2 at each pair of E_T values. As shown, the luminosity and resolution uncertainties are quite significant at low E_T and uncertainties in the jet energy scale dominate at high E_T . Since the luminosity uncertainties are fully correlated over all E_T , as are the resolution uncertainties, and since the energy scale uncertainties at large E_T are also correlated, the overall systematic uncertainty is largely correlated. Table II shows that the bin-to-bin correlations in the full uncertainty for representative E_T bins are greater than 40% and positive. (The full covariance matrix can be found in Ref. [15].)

Table III lists χ^2 values for several JETRAD predictions incorporating various parton distribution functions [4,5]. Each comparison has 24 degrees of freedom. The JETRAD predictions have been fit to a smooth function of E_T . All five predictions describe the $|\eta| \leq 0.5$ cross section very well (the probabilities for χ^2 to exceed the listed values are between 47 and 90%). The $0.1 \leq |\eta| \leq 0.7$ cross section is also well described (probabilities between 24 and 72%). Comparisons for $|\eta| \leq 0.5$ with EKS [1] calculations using CTEQ3M, $\mathcal{R}_{\text{sep}}=1.3\mathcal{R}$, and with renormalization scales $\mu = cE_T^{\text{max}}$ or cE_T^{jet} , where c varies, are shown in Table IV. These calculations also describe the data very well (better than 57% probability) at all renormalization scales.

The top panel in Fig. 4 shows $(D - T)/T$ for our data in the $0.1 \leq |\eta| \leq 0.7$ region relative to an EKS calculation using the CTEQ3M pdf, $\mu = 0.5E_T^{\text{jet}}$, and $\mathcal{R}_{\text{sep}}=2.0\mathcal{R}$. (The tabulated data can be found in Ref. [15].) Also shown are the data of Ref. [8] relative to the same EKS prediction. For this rapidity region, we have carried out a χ^2 comparison between our data and the nominal curve describing the central values of the data of Ref. [8]. Comparing our data to the nominal curve, as though it were theory, we obtain a χ^2 of 63.2 for 24 degrees of freedom (probability of 0.002%). Thus our data cannot be described with this parameterization. As illustrated in the bottom panel of Fig. 4, our data and the curve differ at low and high E_T ; such differences cannot be accommodated by the highly correlated uncertainties of our data. If we include the systematic uncertainties of the data of Ref. [8] in the covariance matrix, the χ^2 is reduced to 24.7 (probability of 46%).

In conclusion, we have made the most precise measurement to date of the inclusive jet

TABLE III. χ^2 comparisons between JETRAD and $|\eta| \leq 0.5$ and $0.1 \leq |\eta| \leq 0.7$ data for $\mu = 0.5E_T^{\max}$, $\mathcal{R}_{\text{sep}}=1.3\mathcal{R}$, and various pdfs. There are 24 degrees of freedom.

pdf	$ \eta \leq 0.5$	$0.1 \leq \eta \leq 0.7$
CTEQ3M	23.9	28.4
CTEQ4M	17.6	23.3
CTEQ4HJ	15.7	20.5
MRSA'	20.0	27.8
MRST	17.0	19.5

TABLE IV. χ^2 comparisons between EKS and $|\eta| \leq 0.5$ data for CTEQ3M, $\mathcal{R}_{\text{sep}}=1.3\mathcal{R}$, and various renormalization scales given by cE_T^{\max} or cE_T^{jet} . There are 24 degrees of freedom.

c	$\chi^2 (E_T^{\max})$	$\chi^2 (E_T^{\text{jet}})$
0.25	14.8	19.8
0.50	19.4	22.2
1.00	16.8	18.1

cross section for $E_T \geq 60$ GeV. QCD predictions are in good agreement with the observed cross section for standard parton distribution functions and different renormalization scales. This is consistent with our previous measurements of dijet angular distributions [14], which are also in good agreement with QCD and show no indication of physics beyond the Standard Model.

We thank the staffs at Fermilab and collaborating institutions for their contributions to this work, and acknowledge support from the Department of Energy and National Science Foundation (U.S.A.), Commissariat à L'Energie Atomique (France), Ministry for Science and Technology and Ministry for Atomic Energy (Russia), CAPES and CNPq (Brazil), Departments of Atomic Energy and Science and Education (India), Colciencias (Colombia), CONACyT (Mexico), Ministry of Education and KOSEF (Korea), and CONICET and UBACyT (Argentina). We thank W. T. Giele, E. W. N. Glover, and D. A. Kosower for help with JETRAD and B. Flaucher for help with data comparisons.

REFERENCES

* Visitor from Universidad San Francisco de Quito, Quito, Ecuador.

† Visitor from IHEP, Beijing, China.

- [1] S. D. Ellis, Z. Kunszt, and D. E. Soper, Phys. Rev. Lett. **64**, 2121 (1990).
- [2] F. Aversa *et al.*, Phys. Rev. Lett. **65**, 401 (1990).
- [3] W. T. Giele, E. W. N. Glover, and D. A. Kosower, Phys. Rev. Lett. **73**, 2019 (1994).
- [4] H. L. Lai *et al.*, Phys. Rev. D **51**, 4763 (1995). H. L. Lai *et al.*, Phys. Rev. D **55**, 1280 (1997).
- [5] A. D. Martin *et al.*, hep-ph/9803445, to appear in Eur. Phys. J. C (1998).
- [6] S. Abachi *et al.* (DØ Collaboration), Nucl. Instr. Meth. Phys. Res. A **338**, 185 (1994).
- [7] J. Alitti *et al.* (UA2 Collaboration), Phys. Lett. B**257**, 232 (1991); Z. Phys. C **49**, 17 (1991). F. Abe *et al.* (CDF Collaboration), Phys. Rev. Lett. **70**, 1376 (1993).
- [8] F. Abe *et al.* (CDF Collaboration), Phys. Rev. Lett. **77**, 438 (1996).
- [9] B. Abbott *et al.* (DØ Collaboration), Fermilab-Pub-97-242-E (1997).
- [10] V.D.Elvira, Ph. D. Thesis, Universidad de Buenos Aires, 1995 (unpublished), http://www-d0.fnal.gov/results/publications_talks/thesis/thesis.html
- [11] B. Abbott *et al.* (DØ Collaboration), Submitted to Nucl. Instr. Meth. Phys. Res. A, (1998) Fermilab-Pub-97/330-E.
- [12] M. Bhattacharjee, Ph. D. Thesis, University of Delhi, 1996 (unpublished).
- [13] B. Abbott *et al.*, hep-ph/9801285, to appear in Eur. Phys. J. C (1998).
- [14] B. Abbott *et al.* (DØ Collaboration), Phys. Rev. Lett. **80**, 666 (1998).
- [15] Covariance matrices and $0.1 \leq \eta \leq 0.7$ data will be available from the AIP E-PAPS service and at <http://www-d0.fnal.gov/~d0qcd/inclusive>.

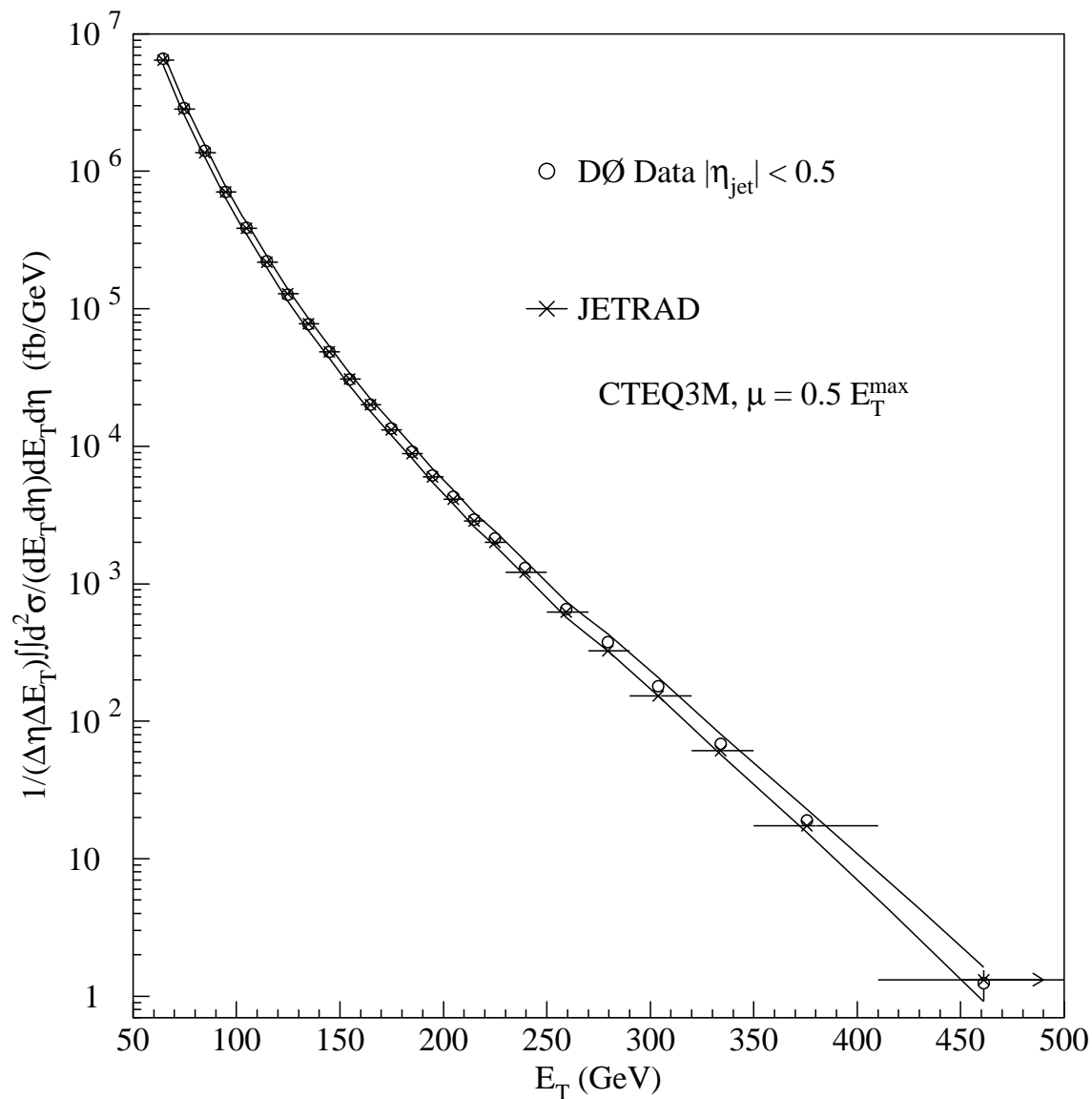


FIG. 1. The $|\eta| \leq 0.5$ inclusive cross section. Statistical uncertainties are invisible on this scale. The solid curves represent the $\pm 1\sigma$ systematic uncertainty band.

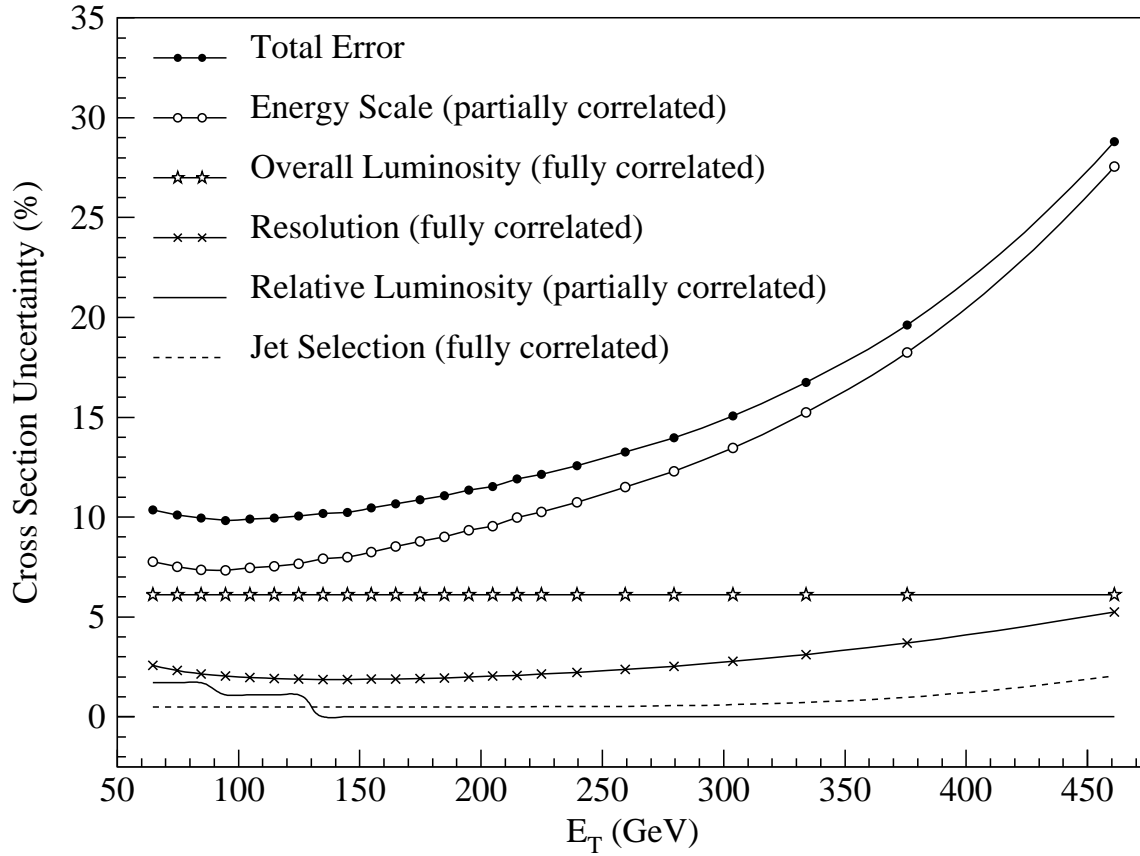


FIG. 2. Contributions to the $|\eta| \leq 0.5$ cross section uncertainty plotted by component.

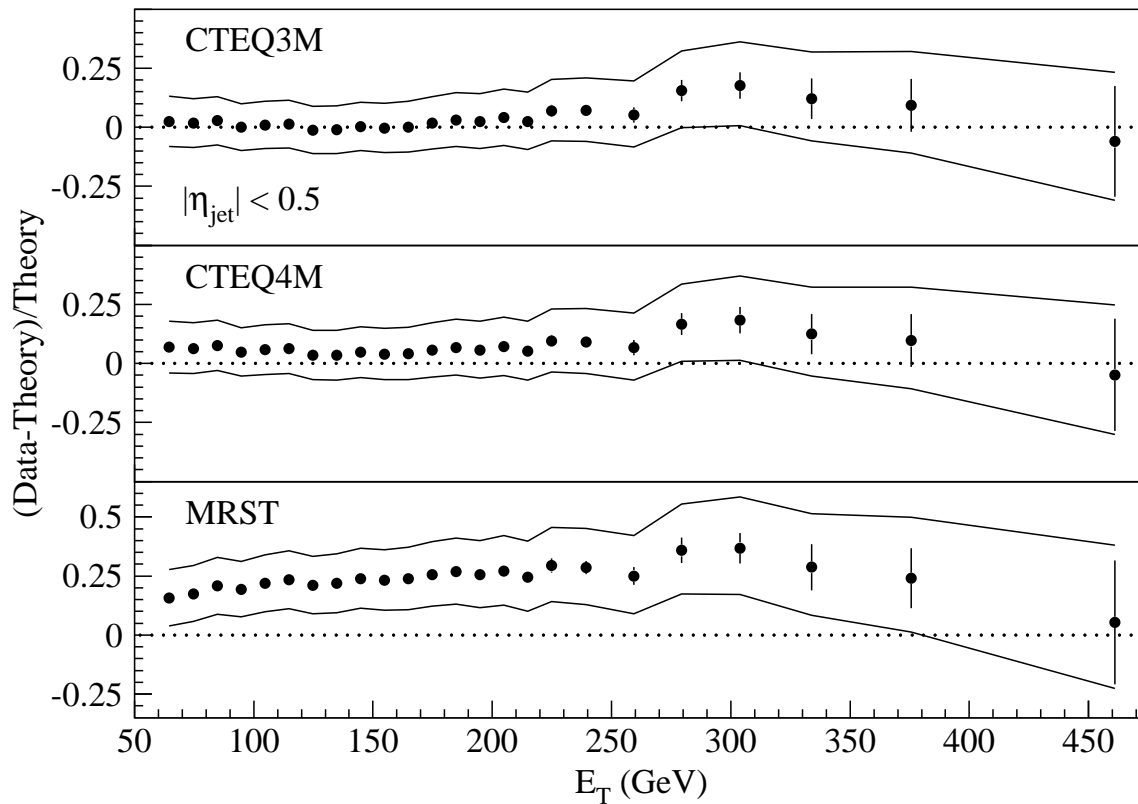


FIG. 3. The difference between data and JETRAD QCD predictions normalized to predictions. The bands represent the total experimental uncertainty.

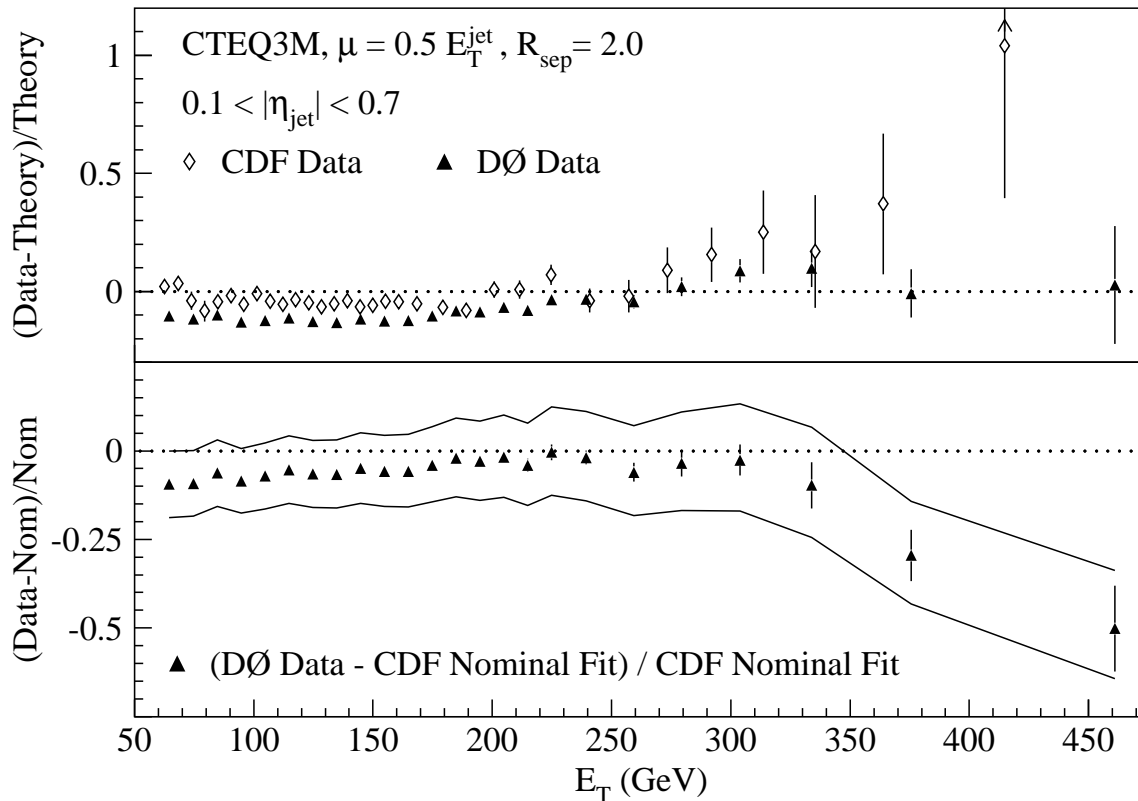


FIG. 4. Top: Normalized comparisons of our data to EKS and of the data in Ref. [8] to EKS. Bottom: Difference between our data and smoothed results of Ref. [8] normalized to the latter. The band represents the uncertainty on our data.